a reprint from Applied Optics

Prototype Michelson interferometer with Fabry–Perot cavities

David Shoemaker, Peter Fritschel, Joseph Giaime, Nelson Christensen, and Rainer Weiss

We describe a rigid, internally modulated Michelson interferometer with Fabry–Perot cavities in the interferometer arms. The high contrast (0.986) and the small cavity losses (2.7%) permit efficient use of the light power available. The measured shot-noise-limited displacement sensitivity for 35 mW of light power is 2.5×10^{-17} m$\sqrt{\text{Hz}}$, in good agreement with the calculated signal-to-noise ratio. *Key words:* Interferometry, Michelson, Fabry–Perot, techniques for gravitational radiation detection.

I. Introduction

Interferometric measurements of small displacements have a number of applications, among them the detection of gravitational radiation (Refs. 1 and 2 and references therein). Techniques for increasing the sensitivity of such measurements involve increases in the effective light power through higher laser power[3,4] or recycling,[5] squeezing of the light field,[6] and folding the light path in the arms of the interferometer. Two folding methods are favored: the Herriott delay line[7] and the Fabry–Perot cavity. As part of the research and development program in support of the Caltech/MIT Laser Interferometer Gravitational Wave Observatory project,[8] we built a small, rigid, prototype Michelson interferometer with Fabry–Perot cavities in the arms to determine realistic parameters for, and to aid in the design of, full-scale interferometers. Several free-mass prototype gravitational wave detectors have been built with Fabry–Perot cavities,[9,10] but these do not employ optically recombined beams from the two orthogonal arms. Earlier efforts at rigid recombined-beam interferometers have not employed state-of-the art optics[11] or cavity finesses similar to those to be used in the full-scale antennas[10] and have not illuminated some critical points for the extrapolation to a full-scale system.

We chose to perform this research on a rigid, fixed-mass interferometer at atmospheric pressure because it allows us to concentrate our attention on the optical configuration. The complexities associated with suspended, seismically isolated masses are avoided. One of the implications of this approach, however, is that our measurements must be made at frequencies higher than ambient acoustic and mechanical excitations. Thus the target measurement frequency for this research is 80 kHz, whereas the full-scale interferometers are sensitive in the region around 1 kHz.

In this paper we describe the optical system and its static characteristics (contrast, losses, etc.), the servo systems and synchronous modulation fringe detection, and finally the sensitivity of the complete interferometer and its limits.

II. Optics

A. Layout

The layout is shown in Fig. 1. The interferometer is constructed with commercial mirror mounts on small optical tables bolted to the circular bottom plate of a 1.5-m diam vacuum tank. This bottom plate is isolated from seismic ground motion with rubber-damped springs, giving horizontal and vertical resonances of ≈4 Hz. The vacuum tank is closed, but not pumped out, during the experiment. The entire tank is overpressured with filtered air. The cavity mirrors and the space between them are protected by glass tubes filled with very clean (filtered to 0.1-μm particle size with 99.99% efficiency) boiloff from liquid N_2 or with He gas. Sound absorbing material (Sonex 1) inside the tank is used to absorb acoustic noise.

Light from the laser (which is on a separate table) is coupled into a single-mode fiber, and this fiber is led into the vacuum system and is terminated in the block labeled fiber–grin; the output of this fiber–grin lens assembly is a nearly collimated beam. It is mode matched to the Fabry–Perot (FP) cavities with a single positive lens and isolated by two Faraday isolators in series. The light falls on a disk beam splitter (BS) and

The authors are with the Department of Physics and Center for Space Research, Massachusetts Institute of Technology, Cambridge, Massachusetts 02139.

Received 13 June 1990.
0003-6935/91/223133-06$05.00/0.

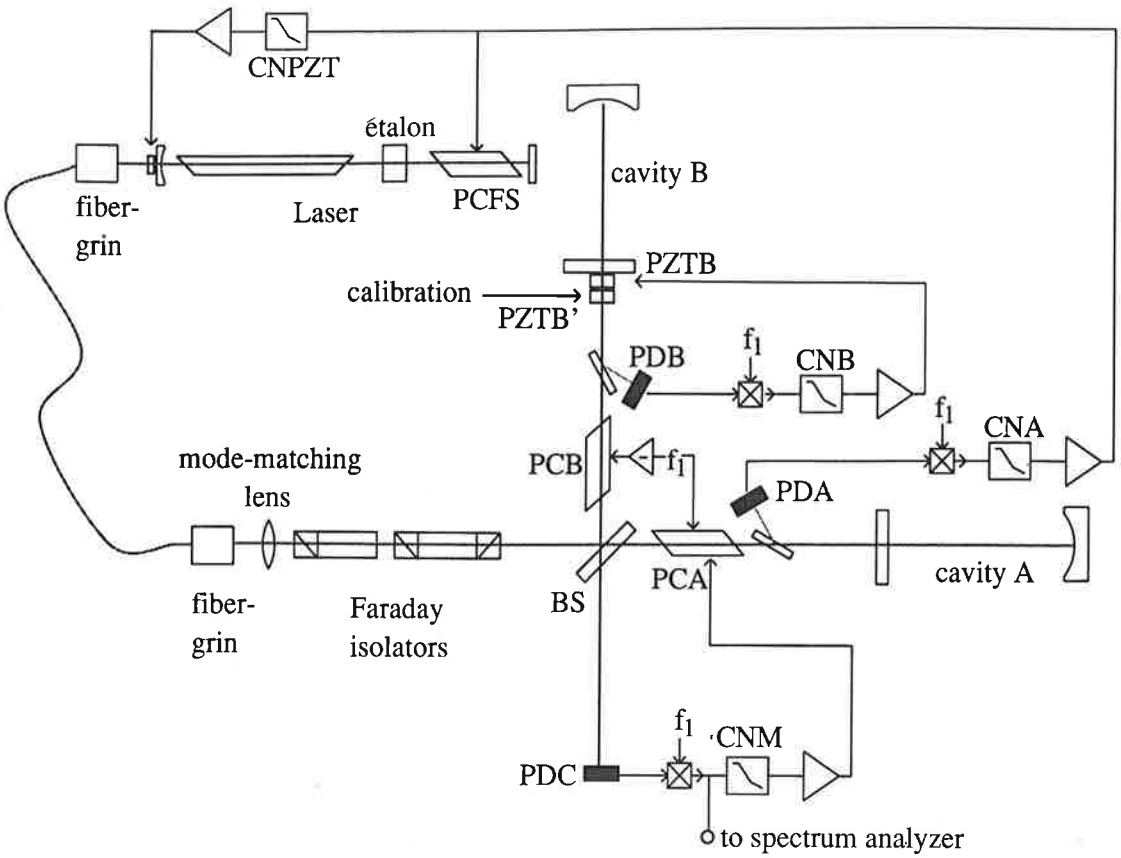

Fig. 1. Schematic diagram of the interferometer.

is sent (in each arm) through a Pockels cell (PCA and PCB in the figure) and into the 47-cm long FP cavity. A small part (3%) of the reflected light is sent to a photodiode (PDA or PDB); the rest returns to the beam splitter where it interferes with the light from the other arm. The light leaving the antisymmetric port of the interferometer falls on the third photodiode (PDC) in the system. The light leaving the interferometer through the symmetric port (coincident with the incoming light) is rejected by the middle polarizing beam splitter (CNM) in the Faraday–isolator assembly.

B. Measured Optical Characteristics

The Ar^+ laser (Spectra-Physics 2020) has a wavelength selective output coupler for the 514.5-nm line and an étalon for single-longitudinal-mode operation. With the intracavity Pockels cell that is used for frequency stabilization, the laser has ≈0.5-W maximum output (0.85 W without Pockels cell). The overall optical efficiency of the light delivery system from the laser output to the interferometer beam splitter is 0.3 (0.5 from the fiber coupler; 0.6 from the assorted lenses and Faraday isolators).

The FP cavities themselves are made up of superpolished mirrors (polished by Optics Technology and coated by particle-measurement systems). The input coupling mirror is flat, and the rear mirror has a 1-m radius. The transmission of the input coupling mirror is 2.8%, and thus the finesse is ≈220, and the linewidth 1.4 MHz. By looking at the transmitted light though the cavity as it is swept in length through a free spectral range, the mode matching can be determined: the intensity of the light in the TEM_{00} mode can be compared with the sum of the intensities in all the modes. We measure a mode matching efficiency (in intensity) of $M = 0.95$. The reflectivity of the cavity on-resonance is 97.5% (corrected for the finite matching), which allows us to infer the total losses in the cavity to be 160 ppm. Particle-measurement systems had quoted losses for the rear mirror of 52 ppm (of which 17 ppm are due to transmission), and thus we believe that the input coupling mirror has losses of ≈110 ppm. To the precision of our measurements (approximately ±5%), we see no difference between the two cavities in terms of the matching, finesse, or losses. We have seen no degradation of the mirror characteristics over a one-month period, and thus our precautions in providing a clean environment appear to be sufficient.

The far mirrors of the FP's can be blocked, leaving a simple Michelson interferometer (MI). The contrast of this interferometer, without Pockels cells in place, is $C = (I_{max} - I_{min})/(I_{max} + I_{min}) = 0.996$; with the Pockels cells (Gsänger PM-25) in place, the contrast becomes $C = 0.989$ (which we believe is primarily the result of one particular Pockels cell that shows excessive scattering). With the FP cavities locked, the contrast is $C = 0.986$. This last figure may be limited by our current

ability to align the system; remote controls (PZT's) and misalignment information (phase front analysis) are necessary to determine the intrinsic limits.

III. Servo and Measurement Systems

Synchronous modulation–demodulation at $f_1 = 5.38$ MHz is used to detect the lengths of the two cavities (by means of the reflected light) and the Michelson fringe (by means of the light leaving the antisymmetric port). The modulation is impressed on the laser light by the Pockels cell (PCA, PCB) in each arm of the interferometer. The laser frequency is stabilized to the length of cavity A, cavity B is held on resonance by means of an actuator PZTB mounted on one of the cavity mirrors, and the Michelson is held on the dark fringe through voltages applied (in addition to the modulation) to the Pockels cells.

A. Frequency Stabilization

The laser is stabilized to cavity A using the reflection technique.[12] An error signal is derived by demodulating a fraction of the reflected light with 5.38 MHz. It is sent through a servo compensation network (CNA), which is a simple pole at 100 Hz for initial locking; for normal operation, another pole–zero pair (100 Hz and 100 kHz) is used. Finally, a Sallen–Key circuit can be added to give extra gain in the vicinity of 80 kHz (at the expense of a reduced gain around 40 kHz). The signal is amplified by a high-frequency high-voltage (±85 V) amplifier and applied to a Pockels cell (PCFS) in the laser cavity. The unity-gain frequency is ≈700 kHz with a simple pole as compensation; with the normal compensation filter in place, the unity-gain frequency is ≈300 kHz. Long-term drifts are countered by a second loop (with compensation CNPZT) using a piezoelectric transducer actuator on the laser output coupling mirror.

B. Arm B Cavity Locking

The second arm is locked to the stabilized laser light frequency with the same reflection and demodulation technique as above. The basic servo compensation (CNB) is similar to that for cavity A, except that the pole–zero pair for the normal operating condition is at 1 Hz and 3 kHz. The actuator for the servo system is a piezoelectric transducer (PZTB) on the input coupling mirror of cavity B, which has a pronounced (24 kHz, $Q = 15$) resonance; to allow a higher unity-gain frequency in the servo loop, a passive antiresonance circuit in the compensation network (CNB) is used to cancel this resonance. The unity-gain frequency thus achieved is 4.5 kHz, which is sufficient to make the excursions from the cavity resonance acceptably small.

With the normal light intensities used for measurements, the unity signal-to-noise (shot and electronic noise limited) for the frequency detection is ≈0.3 Hz/$\sqrt{\text{Hz}}$. For frequencies between 6 and 100 kHz, the gain in the servo loop is sufficient to hold the frequency noise to <1 Hz/$\sqrt{\text{Hz}}$; with the Sallen–Key circuit in place, the frequency noise at 80 kHz is held to the shot-noise limit of 0.3 Hz/$\sqrt{\text{Hz}}$.

C. Michelson Locking and Detection

The Michelson path-length difference is modulated by the same Pockels cells that are used to apply the modulation to the cavities. However, the level of the modulation is significantly reduced by the optical arrangement that has light passing two times through the Pockels cells.

In the first pass through the Pockels cells, the carrier has two sidebands at $\pm f_1 = \pm 5.38$ MHz put on it. This falls on a cavity; the sidebands are largely outside the resonance curve of the FP, and thus are shifted by ≈0 and 2π rad after reflection. The carrier, which is held on the cavity resonance, is shifted by π rad after reflection. The reflected light now undergoes a second interaction with the modulator; new sidebands are put on the reflected carrier, which are out of phase with the sidebands that were put on in the first pass through. Thus, there is a cancellation of the modulation.

The quality of the cancellation is a function of several parameters. First, the visibility of the cavity fringes: in the current cavities, all but 2.5% of the light is reflected. The linewidth of the cavity compared to the modulation frequency is relevant; for the FP cavities and 5.38-MHz modulation, the two reflected sidebands are not at 0° and 360° but at 13° and (360° − 13°). Finally, the distance between the modulator and the cavity input coupling mirror: the transit time causes an additional phase shift between the original and second sidebands, contributing ≈3° of phase delay. A calculation shows the ratio of the signal at the modulation frequency in the double-passed configuration I^{dp} to the signal for a single pass through the modulator I^{sp} to be

$$\frac{I^{\text{dp}}(\omega_m)}{I^{\text{sp}}(\omega_m)} = J_0^2(\Gamma)\{(1-\sqrt{A})^2 + [\sin(2\omega_m l/c + \phi_{\text{cav}})]^2\}^{1/2}.$$

This is derived for the case of unity contrast. Here Γ is the modulation index for a single pass through the modulator, A is the intensity reflection coefficient of the cavity on-resonance, l is the distance from the modulator to the cavity, and ϕ_{cav} is the phase shift added to the $\omega_0 \pm \omega_m$ sidebands after reflection from the cavity. In our case, the amplitude term, $(1-\sqrt{A})^2 = (1-0.987)^2 = 1.7 \times 10^{-4}$, is very small, and our signal comes almost entirely from the phase shift term, $[\sin(16°)]^2 = 7.6 \times 10^{-2}$. This gives a signal ratio of $I^{\text{dp}}/I^{\text{sp}} = 1/3.7$ for a typical Γ of 0.16. Our observations of this reduction compare the ω_m signal (monitored at the radio frequency output of the PDC) of the FP MI and the one-bounce MI. In the one-bounce MI the modulation is nearly doubled on the second pass, and we would predict a signal ratio, in the region where $J_1(\Gamma)$ is linear with Γ, of $I^{\text{FPMI}}/I^{\text{MI}} = 1/7.4$, which is in fair agreement with our directly observed ratio of 1/9. The result of this cancellation is that the optimum modulation depth in the recombined beam FP MI cannot be reached; note that the cavity lock (for which the signal is picked off before the second pass through the modulator) does not suffer from this cancellation.

However, sufficient signal is available to hold the Michelson to a dark fringe and to make measurements

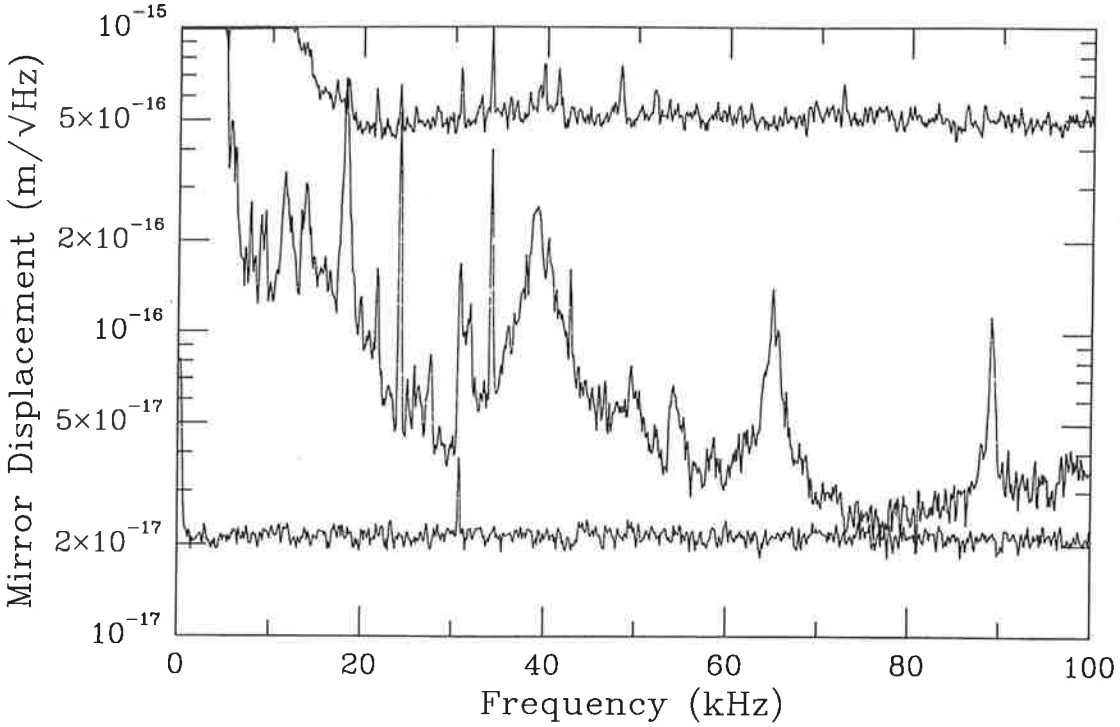

Fig. 2. Interferometer spectrum: top curve, the simple one-bounce Michelson interferometer; middle curve, the recombined-beam FP MI; bottom curve, the shot noise for the recombined-beam Fabry–Perot Michelson measurement.

of the resulting signal-to-noise ratio. The demodulated signal from the photodiode receiving light from the antisymmetric output of the interferometer is put through a compensation network CNM similar to those above, with a pole at 160 Hz for initial locking and a pole–zero pair at 1 Hz and 3 kHz for normal operation. The filtered signal is amplified with a fast high-voltage amplifier and sent to one of the Pockels cells. A unity-gain frequency of 5 kHz is attainable and sufficient. We analyzed the error signal of this loop above the unity-gain frequency to obtain the displacement noise spectrum. It is calibrated in displacement using a second piezoelectric transducer (PZTB′) mounted on the B arm cavity input coupling mirror: the signal for a given applied 35-kHz signal can be seen in both the recombined-beam FP Michelson and in the simple interferometer, where the absolute magnitude can be determined either from the known sensitivity of the Pockels cell or from the calibration signal size directly compared with the Michelson output fringe amplitude.

IV. Signal Sensitivity, Noise Sources

Figure 2 shows the spectrum, expressed as equivalent mirror displacement noise of a single-cavity mirror in $m/\sqrt{Hz}$, of the interferometer. The photocurrent on the Michelson light fringe for these measurements is 8 mA (which corresponds to ≈35 mW of incident light power). The top flat curve is the spectrum of the demodulated signal from the Michelson antisymmetric output of the simple one-bounce Michelson with a modulation depth of $\Gamma = 0.32$; note the lack of features at frequencies above ≈10 kHz. This noise level is at the shot-noise limit for the measurement. This curve assures us that the electronic systems are working correctly.

The spectrum with the two FP cavities locked is the middle, rapidly falling, curve in Fig. 2. At low frequencies (up to 30 kHz) acoustic noise is dominant. This source of noise determines the servo loop characteristics that are required, as it is against these large fluctuations that the system must be held on-resonance or on the dark fringe. In the 30–100-kHz band, a number of resonances can be seen. These are probably thermally driven resonances in the FP cavity mirror supports and are consistent with masses and resonance Q's in the system. This noise source is the practical limit to the obtainable sensitivity with this interferometer constructed of mirrors in conventional mounts. In a full-scale interferometer, the mechanical suspension and isolation of the optical components reduces these noise sources to a level such that at astrophysically interesting frequencies (around 1 kHz) the requisite sensitivity is achieved.

In a region between 70 and 85 kHz, the spectrum closely approaches the shot noise associated with the photocurrent of the measurement. This is determined by replacing the laser light on the antisymmetric photodetector with an incandescent light source that produces the same photocurrent; this results in the noise level shown as the bottom trace in Fig. 2. This corresponds to a sensitivity of $\approx 2.5 \times 10^{-17}$ $m/\sqrt{Hz}$. We note that the increase in sensitivity obtained by adding the cavities is of the order of 25; this sensitiv-

ity is reduced from the ideal factor of $2(\text{finesse})/\pi \approx 140$ because of the reduction in modulation depth discussed above.

We have measured the sensitivity of the complete recombined-beam interferometer to frequency fluctuations of the incoming light to be 2.5×10^{-17} m/Hz. This can be interpreted as a difference in storage times of the two cavities of one part in 2000. The calculated position noise that results, given our frequency noise at 80 kHz of 0.3 Hz/$\sqrt{\text{Hz}}$, is at a level of 7.5×10^{-18} m/$\sqrt{\text{Hz}}$. This is somewhat below the shot-noise-limited position sensitivity of the recombined-beam interferometer of 2.5×10^{-17} m/$\sqrt{\text{Hz}}$.

A thorough calculation of the sensitivity of this instrument that properly takes into account contrast imperfections and the double passing of the modulator is quite involved. However, for small modulation, where $J_1(\Gamma)$ is linear with Γ, the double-passing is approximately equivalent to reducing the modulation depth, and we can use the simple sensitivity formula for a single-passed recombined-beam FP MI, replacing the single-pass modulation index with our reduced index. In the limit where the measurement frequency is small compared to the linewidth $c/2lF$ of the FP cavities in the arms of the interferometer, for sensitivity $\tilde{x}$, where $\tilde{x}$ is the motion of one interferometer mirror, this gives

$$\tilde{x} = \left(\frac{\lambda}{8F}\right)\left(\frac{2e}{I_{\max}+I_{\max}}\right)^{1/2} \times \left\{\frac{[1 - CJ_0(2\Gamma_{\text{net}}) + 2I_{\text{det}}/(I_{\max} + I_{\min})]^{1/2}}{MJ_0(\Gamma_{\text{net}})J_1(\Gamma_{\text{net}})}\right\}.$$

Here $\lambda = 0.514 \times 10^{-6}$ m is the wavelength of light, F is the arm cavity finesse, e is the electronic charge, and M is the fraction of the incident power that is coupled into the TEM_{00} mode; $I_{\max}$ is the photocurrent on the bright fringe, and $I_{\min}$ is the photocurrent on the dark fringe without modulation, both measured at the interferometer output; I_{det} is the current that would produce a shot noise equal to the electronic noise contribution of the photodiode–amplifier combination; $J_0(\Gamma)$ and $J_1(\Gamma)$ are Bessel functions; the depth of modulation Γ_{net} is the net modulation, after cancellation. To model the interferometer contrast C, the two beams returning from the cavities are analyzed as having interfering and noninterfering components, as would be the case if wave-front distortion were the primary cause of the contrast defect. Spatial analysis of the interferometer output intensity shows that this cause is dominant. Other models for the contrast give negligibly different values for the signal-to-noise ratio.

The first factor in the sensitivity formula is the change in phase of the interferometer arm ϕ for a change in length x of the arm; for our cavities, with a finesse of $F = 220$, this has a value of 2.9×10^{-10} m/rad. The second factor is the phase uncertainty $\tilde{\phi}$ caused by the shot noise of the photocurrent. For the measurement presented here, we have $I_{\max} = 8$ mA and $\tilde{\phi} = 6.3 \times 10^{-9}$ rad/$\sqrt{\text{Hz}}$. The first two factors together give the ideal shot-noise-limited unity signal-to-noise ratio, which for the measurement presented here gives a possible sensitivity of 1.8×10^{-18} m/$\sqrt{\text{Hz}}$. The third factor takes into account the imperfections in the optical and detection systems and has a value of 2 for a perfect system. Given the measured parameters $I_{\text{det}} = 0.016$ mA and $I_{\text{mod}} = 0.220$ mA, the electronic noise caused by the photodiode–amplifier combination is negligible. With the finite contrast ($C = 0.95$ for the measurement presented) but with optimal modulation for this contrast ($\Gamma = 0.54$), the third factor would be 2.42. However, using the largely canceled modulation ($\Gamma_{\text{net}} = 0.036$, which has been reduced by the measured factor of $I^{\text{FPMI}}/I^{\text{MI}} = 1/9$) and the measured contrast gives a factor of 12.6, and thus a predicted sensitivity of 2.3×10^{-17} m/$\sqrt{\text{Hz}}$. This is in good agreement with the measured value.

In a separate experiment to verify the increase in sensitivity because of the FP cavities in the interferometer arms, a fixed-level 60-kHz modulation was applied to the cavity B piezoelectric transducer (PZTB). Cavity A was blocked. With cavity B alternately on-resonance and off-resonance (and thus effectively blocked), the Michelson was swept through several fringes, and the antisymmetric output was demodulated with the 60-kHz modulation frequency. The demodulated signal on-resonance was 143 times greater than with the unlocked cavity, which is in excellent agreement with the expected result. This experiment, which does not suffer the reduction in modulation depth seen with the double-passed modulation scheme, is a direct confirmation of the expected increase in sensitivity to arm length changes when a cavity is used.

V. Conclusion

We have demonstrated a MI with internal modulation and with FP cavity arms with a finesse appropriate to a full-scale interferometer. Its optical characteristics are encouraging: the relatively small losses in the arms, the symmetry between the arms, and the high contrast between the recombined beams indicate that some aspects of the mirror technology for the full-scale interferometers are close at hand. The shot-noise-limited sensitivity of the interferometer, 2.5×10^{-17} m/$\sqrt{\text{Hz}}$, agrees well with the calculated sensitivity for the experimental parameters.

The modulation technique used here, while convenient for initial prototyping efforts, has several disadvantages, the most important being that electro-optic modulators introduce contrast defects and cannot withstand the desired power levels in recycled interferometers without introducing considerable beam distortion. In addition, cancellation of the modulation in the Michelson reduces the sensitivity and complicates the interpretation of our experimental arrangement. A longer path length between the modulator and the cavity input mirror (of the order of 14 m for our present modulation frequency $f_1 = 5.38$ MHz) would provide a solution to the cancellation of modulation sidebands, but an alternative modulation scheme such as external modulation[13,14] is a more attractive and complete solu-

tion. However, the in-line modulation system is a convenient starting point: there is substantial convenience in the optical simplicity of the scheme and the ease of phase control with the internal Pockels cells.

D. Shoemaker thanks D. Dewey and K. Strain for helpful discussions. This study is supported by National Science Foundation grant PHY-8803557.

References

1. R. Weiss, "Electromagnetically coupled broadband gravitational antenna," MIT Res. Lab. Electron. Q. Prog. Rep. **105,** 54–76 (1972).
2. B. Buckingham, ed., *Proceedings of the Fifth Marcel Grossmann Meeting on General Relativity, Perth, 1988* (World Scientific, Singapore, 1989).
3. O. Crégut, C. N. Man, D. Shoemaker, A. Brillet, A. Menhert, P. Peuser, N. P. Schmidt, P. Zeller, and K. Wallmeroth, "18 W single frequency operation of an injection-locked, cw, Nd:YAG Laser," Phys. Lett. A **140,** 294–298 (1989).
4. C. Nabors, A. Farina, T. Day, S. Yang, E. Gustafson, and R. Byer, "Injection locking of a 13-W cw Nd:YAG ring laser," Opt. Lett. **14,** 1189–1191 (1989).
5. R. Drever, "Interferometric Detectors for Gravitational Radiation," in *Gravitational Radiation*, N. Deruelle and T. Piran, eds. (North-Holland, Amsterdam, 1983), pp. 321–338.
6. M. Xiao, L. Wu, and H. Kimble, "Precision Measurement Beyond the shot-noise limit," Phys. Rev. Lett. **59,** 278–281 (1987).
7. D. Herriott, H. Kogelnik, and R. Kompfner, "Off-axis paths in spherical mirror interferometers," Appl. Opt. **3,** 523–526 (1964).
8. R. Vogt, "The LIGO project—a progress report," presented at the Twelfth International Conference on General Relativity and Gravitation, Boulder, Colo., 1989.
9. R. Spero, "Status report on the Caltech 40-meter Fabry-Perot prototype gravitational wave detector," presented at Twelfth International Conference on General Relativity and Gravitation, Boulder, Colo., 1989.
10. B. Meers, "Status report on the Glasgow 10-meter Fabry-Perot prototype gravitational wave detector," presented at Twelfth International Conference on General Relativity and Gravitation, Boulder, Colo., 1989.
11. A. Brillet, "Progress at Orsay," presented at Second European Workshop on Gravitational Wave Detection, Chantilly, France, 1986.
12. R. Drever, J. Hall, F. Kowalski, J. Hough, G. Ford, A. Munley, and H. Ward, "Laser phase and frequency stabilization using an optical resonator," Appl. Phys. **31,** 97–105 (1983).
13. R. Drever, "Prospects for laser interferometer gravitational radiation detectors," presented at Tenth International Conference on General Relativity and Gravitation, Padova, Italy, 4–9 July 1983.
14. N. Man, D. Shoemaker, M. Pham Tu, and D. Dewey, "External modulation technique for sensitive interferometric detection of displacements," Phys. Lett. A **148,** 8–16 (1990).